DOI: 10.1002/ejic.200900865

NMR Chemical Shifts of Metal Centres in Polyoxometalates: Relativistic DFT Predictions

Nina Vankova,*[a,b] Thomas Heine,[a] and Ulrich Kortz[a]

Keywords: Density functional calculations / NMR spectroscopy / Polyoxometalates / Vanadium / Tungsten

A DFT approach incorporating relativistic corrections and solvent effects was tested for NMR calculations on transition-metal centres in polyoxometalates. For a monoplatinum decavanadate derivative and a set of dilacunary polyoxotungstates ^{51}V and ^{183}W chemical shifts were calculated at several levels of theoretical treatment regarding solvent, counterion and exchange-correlation functional. Calculations were performed first in the gas phase to model isolated ions and next in a continuum model for water to evaluate the importance of solvation for the quality of the computed chemical shifts. We show that the use of the orbital-dependent Kohn–Sham exchange-correlation functional SAOP in ZORA spin-orbit calculations with solvent effects included via COSMO substantially improves the agreement between computed results and experimental benchmarks for ^{51}V chemical shifts (at least, in the case of $[H_2Pt^{IV}V_9O_{28}]^{5-}$). In the case of dilacunary polyoxotungstates our calculations confirm the necessity of modelling an ion pair in which a counterion is specifically included in the POM lacuna to attain accurate predictions of the corresponding ^{183}W NMR spectra. We show that if the counterion is relatively small (like Li^+ and Na^+), the explicit location of a water molecule in its vicinity (in addition to the overall COSMO treatment) improves further the accuracy of the correlation between computed and experimental shifts (to less than 5 ppm of the encompassed δ range).

Introduction

Over the last few years, the chemistry of polyoxometalates (POMs) has continued its rapid development not only as a pure chemical science, but in a multidisciplinary manner as well, interacting with other areas such as catalysis, surfaces, magnetism, bio- and nanotechnology, medical and materials science.[1,2] The permanent interest in POM chemistry is largely due to the versatile nature of POMs, in terms of their structure, size, redox activity, solubility, thermal stability and charge density. POMs are polynuclear anions composed of edge- and corner-shared metal–oxygen octahedra, forming a compact framework.[3] They have the general formula $[X_xM_mO_y]^{q-}$, in which X is usually a main-group element (e.g., H, P, Si, Ge, As), and the transition metal M is typically Mo, W or V.[4] Partial substitution of Mo, W or V by other transition metals (e.g., Pd, Pt, Au), lanthanides, organic or organometallic groups yields mixed derivatives with interesting properties.[2,3,5]

A powerful method for structural characterization of POMs is heteronuclear magnetic resonance spectroscopy.[6] By displaying sets of chemical shifts sensitive to structure, solvent and counterions, NMR provides essential information on the POM solution state, though the assignment of the recorded spectra is often not straightforward.

Despite the steady advancement in NMR techniques, heteronuclear magnetic resonance is hampered by some serious difficulties, such as very low sensitivity (i.e., small magnetogyric ratio) of the active isotopes (e.g., ^{183}W, ^{99}Ru),[4,7] high quadrupole moment of nuclei like ^{51}V and ^{99}Ru[7,8] or chemical shift anisotropy (as for ^{183}W, ^{195}Pt),[9,10] the latter two providing efficient relaxation pathways leading to broadened spectral lines and a correspondingly low signal-to-noise ratio (S/N). Whereas the experimental NMR spectra of simple POMs can often be assigned just on the basis of relative intensities of the signals as the only source of information, this may not be the case for POMs with low symmetry, featuring between 6 and 11 individual spectral lines.[4] Furthermore, chemical shifts of many heteronuclei span thousands of parts per million (ppm) and respond to structural changes in a counterintuitive manner.[11] Consequently, there is a need for supplementary methodologies that may help NMR spectroscopists to assign such spectra, even under unfavourable conditions and without prior empirical knowledge.

[a] School of Engineering and Science, P.O. Box 750 561, Jacobs University Bremen,
28725 Bremen, Germany
Fax: +49-421-200-49-3223
E-mail: n.vankova@jacobs-university.de
[b] Faculty of Chemistry, University of Sofia,
1 James Bourchier Ave., 1164 Sofia, Bulgaria

Supporting information for this article is available on the WWW under http://dx.doi.org/10.1002/ejic.200900865.

In this respect, quantum chemical calculations represent a powerful tool, allowing meaningful predictions of the main NMR properties (chemical shifts and coupling constants) of many NMR-active nuclei, which can be used for spectral assignment of the experimental data. Modelling the NMR properties, however, has proved to be particularly demanding, as an accurate description of the electron density in the very vicinity of the nucleus is mandatory. Considering POMs, with the view of heavy nuclei involved, computations are even more challenging due to the large number of electrons occupying shells with high angular momentum (such as *f* orbitals) and the associated relativistic effects that have a remarkable influence on all molecular orbitals.[12] Moreover, many such systems exhibit a complex electronic structure with several closely spaced energy levels.[8] The task is even more complicated because POMs are negatively charged polyions and their spectra are usually obtained in polar solvents, which result in significant modification of the electronic structure, and hence of the NMR properties, due to polarization effects caused by counterions and solvent.[4,13]

Despite the difficulties mentioned above, a rapid progress in the field of computational NMR of heavy nuclei has been made in the recent years.[14–16] The comprehensive treatment of heavy atoms, that is, by taking into account the large number of electrons, relativistic effects and accurate description of core shells, is met by the Amsterdam density functional (ADF) code,[17] where a consistent implementation of density-functional theory (DFT) with Slater basis sets, relativistic corrections [scalar relativistic within the zeroth-order regular approximation (ZORA) and spin–orbit corrections] allows a meaningful and informative computation of shieldings and couplings even for atoms as heavy as tungsten, mercury or lead.[18,19] Inclusion of solvent effects, so important in the case of charged species such as POMs, is ensured by the ADF implementation[20] of the conductor-like screening model (COSMO).[21]

In this paper we report on the successful application of DFT incorporating corrections for relativistic and solvent effects for modelling ^{51}V and ^{183}W NMR spectra of POMs of two different types: (1) heterosubstituted polyoxovanadates, represented by the monoplatinum(IV) decavanadate derivative $[H_2Pt^{IV}V_9O_{28}]^{5-}$ and (2) polyoxotungstates of the Keggin dilacunary structure $[\gamma\text{-}XW_{10}O_{36}]^{8-}$, where *X* is Ge or Si. The calculated chemical shifts were compared to experimental values known from the literature[5,22,23] to assess the performance of the adopted DFT protocol. For the whole set of POMs considered, calculations were performed first in the gas phase to model isolated ions and next in a continuum model for water to evaluate the importance of solvation effects for the quality of the computed results. For calculation of ^{51}V chemical shifts, we tested the orbital-dependent exchange-correlation functional SAOP[25] and demonstrated its much better performance regarding the accuracy of the computed results, as compared to conventional GGA functionals commonly used for NMR calculations. In the case of the lacunary polyoxotungstates, we located explicitly an alkali–metal cation (*M* = Li^+, Na^+, K^+) within the lacuna of the polyanion, thus modelling the respective salt $[\gamma\text{-}MXW_{10}O_{36}]^{7-}$, and the resulting effect of the counterion on the ^{183}W NMR spectrum. We assess the performance of the adopted DFT protocol with respect to experimental data by (1) the "mean absolute error" (MAE),[4] defined as the mean value of the absolute difference between calculated and experimental chemical shifts, and (2) the statistical error (*RSE*) of the best correlation between calculation and experiment for the POMs under consideration (see the Computational Details section for the used definition of *RSE*).

This paper is organized as follows: The results from the performed calculations and their comparison with experimental data (as far as available for the POMs of interest) are presented and discussed in the next section. This work is then summarized. The computational procedure in view of combinations of methods, basis sets and treatment of relativistic and solvent effects is described last (see the Experimental Section).

Results and Discussion

The investigated POMs are depicted in Figure 1. It should be noted that the geometries optimized in "continuum water" (by means of COSMO) exhibit shorter bond lengths than those optimized in the "gas phase" for all the POMs considered. As reported previously,[4] hydration causes shrinkage of the overall size of the polyanions, which, though rather small (ca. 1.2% in the case of $[H_2Pt^{IV}V_9O_{28}]^{5-}$ and 1% for the $[\gamma\text{-}MXW_{10}O_{36}]^{7-}$ species), is sufficient to induce marked changes in the calculated shieldings, thus affecting the general performance of the calculations, as described below. Data for both computed and experimental chemical shifts, as determined for the POM structures considered, are summarized in Table 1.

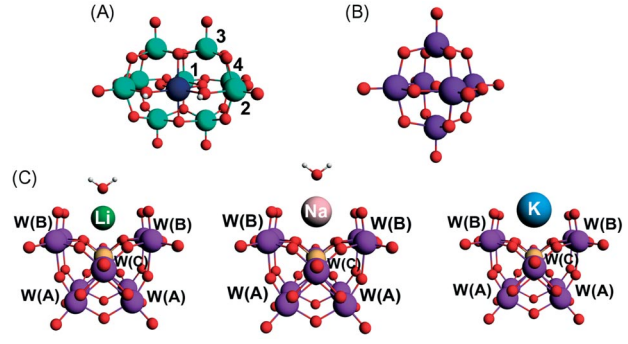

Figure 1. Representative structures of the POMs studied in this work (geometries optimized at *BP/ZORA scalar/Basis II/COSMO level*). (A) $[H_2Pt^{IV}V_9O_{28}]^{5-}$ (PtV9) and the numbering scheme of the vanadium atoms; (B) $[W_6O_{19}]^{2-}$ (W6O19); (C) polyoxotungstates of the type $[\gamma\text{-}MXW_{10}O_{36}]^{7-}$ and the notation scheme of the tungsten atoms, with X = Si or Ge, and M = Li^+, Na^+ or K^+. V: pale green; O: red; Pt: dark blue; H: white; W: violet; Ge or Si: yellow; Li^+: green; Na^+: pink; K^+: blue. Structures optimized at the "gas-phase" level are visually indistinguishable. See the Supporting Information for Cartesian coordinates. Images generated with the ADF view package.

Table 1. Calculated and experimental NMR chemical shifts, δ, for the studied POMs. (A): $\delta(^{51}V)$ in $[H_2Pt^{IV}V_9O_{28}]^{5-}$; NMR reference $VOCl_3$. Gas phase and COSMO calculations at *ZORA spin-orbit/Basis I* level using BP or SAOP functional. (B) and (C): $\delta(^{183}W)$ in $[\gamma\text{-}MXW_{10}O_{36}]^{7-}$, where X = Si or Ge, and M = Li^+, Na^+ or K^+; NMR reference $[W_6O_{19}]^{2-}$. Gas phase-calculations (*BP/ZORA spin-orbit/Basis II/Gas*) presented in (B) and COSMO-calculations in water (*BP/ZORA spin-orbit/Basis II/COSMO*) presented in (C).

(A)

Nuclei numbering	Relative intensity	Calculated ^{51}V δ [ppm] at ZORA spin-orbit/Basis I			Experimental ^{51}V δ [ppm][b]
		Gas phase	Aqueous phase (COSMO)		
		BP	BP	SAOP	
V(1)	1	–210.52	–258.23	–362.77	–368.3
V(2)	2	–264.38	–334.92	–435.89	–443
V(3)	4	–261.12	–329.02	–427.94	–446.9
V(4)	2	–312.84	–373.75	–453.72	–471.15
MAE[a]		170 ppm	108 ppm	12 ppm	

(B)

POM	*M*	Calculated ^{183}W δ [ppm] w.r.t.W6O19			Experimental ^{183}W δ [ppm][c]					
		BP/ZSO/Basis II/Gas			w.r.t.W6O19			w.r.t.WO4		
		W(A)	W(B)	W(C)	W(A)	W(B)	W(C)	W(A)	W(B)	W(C)
$[\gamma\text{-}GeW_{10}O_{36}]^{8-}$	–	–60.12	–83.79	–126.96	–138.9	–174.8	–203.8	–80	–115.9	–144.9
$[\gamma\text{-}MGeW_{10}O_{36}]^{7-}$	K^+	–73.07	–103.80	–136.10						
$[\gamma\text{-}MSiW_{10}O_{36}]^{7-}$	Li^+	–94.02	–122.79	–155.58	–165.8	–206.8	–222.5	–106.9	–147.9	–163.6
	Na^+	–86.90	–114.64	–158.96	–161.2	–202.7	–221.7	–102.3	–143.8	–162.8
	K^+	–93.48	–121.99	–154.46	–155.3	–196.1	–217.1	–96.4	–137.2	–158.2

(C)

POM	*M*	Calculated ^{183}W δ [ppm] w.r.t.W6O19			Experimental ^{183}W δ [ppm][c]					
		BP/ZSO/Basis II/COSMO			w.r.t.W6O19			w.r.t.WO4		
		W(A)	W(B)	W(C)	W(A)	W(B)	W(C)	W(A)	W(B)	W(C)
$[\gamma\text{-}GeW_{10}O_{36}]^{8-}$	–	–142.18	–196.71	–215.94	–138.9	–174.8	–203.8	–80	–115.9	–144.9
$[\gamma\text{-}MGeW_{10}O_{36}]^{7-}$	K^+	–135.49	–183.54	–209.00						
$[\gamma\text{-}MGeW_{10}O_{36}]^{7-}$	$(H_2O)K^+$	–143.45	–190.48	–212.08						
$[\gamma\text{-}MSiW_{10}O_{36}]^{7-}$	Li^+	–156.41	–198.95	–224.22	–165.8	–206.8	–222.5	–106.9	–147.9	–163.6
	$(H_2O)Li^+$	–164.65	–208.17	–228.33						
	Na^+	–154.65	–193.00	–229.76	–161.2	–202.7	–221.7	–102.3	–143.8	–162.8
	$(H_2O)Na^+$	–163.89	–202.09	–237.53						
	K^+	–157.17	–203.12	–226.09	–155.3	–196.1	–217.1	–96.4	–137.2	–158.2
	$(H_2O)K^+$	–166.03	–209.82	–233.28						

[a] Mean absolute error defined as the mean value of the absolute difference between experimental and calculated chemical shifts.[4] [b] Experimental δ values relative to $VOCl_3$ as in ref.[5] [c] Experimental δ values relative to the value for $[W_6O_{19}]^{2-}$ (δ = 58.9 ppm[4]) or to Na_2WO_4 as in ref.[22,23]

Monoplatinum(IV) Decavanadate Derivative

The polyanion $[H_2Pt^{IV}V_9O_{28}]^{5-}$, representing the first platinum(IV)-containing polyoxovanadate, was synthesized and experimentally characterized by Lee and Kortz.[5] In the discussion further on, for the sake of brevity, we denote it as PtV9. PtV9 has C_{2v} symmetry and exhibits four non-equivalent vanadium atoms (see the numbering scheme in Figure 1A) corresponding to four individual peaks in the experimental ^{51}V NMR spectrum. The peaks span a δ range of 103 ppm and their assignment was done on the basis of their relative intensities 1:2:4:2, as well as on structural considerations.[5]

We run "gas phase" and "aqueous phase" (i.e., COSMO) calculations at *ZORA spin-orbit/Basis I* level by using either GGA-BP or model SAOP functional. The computed chemi-

cal shifts are listed in Table 1A, along with the corresponding experimental values. The calculation modelling an isolated ion (gas phase in both geometry optimization and shielding computation) produces a spectrum in which all vanadium nuclei are strongly deshielded as compared to the experimental results, and the mean absolute error of δ is quite large (MAE = 170 ppm).

The inclusion of solvent effects by COSMO (in both geometry and NMR calculations), while employing the same (BP) functional as in the gas-phase case, leads to only a slight improvement in the calculated δ values. A major improvement is attained when the COSMO calculations of nuclear shieldings are performed by using the model SAOP functional instead of BP. As seen from Table 1A, this level of theoretical treatment, which is the highest one adopted here, reduces the MAE by almost 90% (from 108 to 12 ppm) and results in an excellent correlation line ($\delta_{calcd.} = a\delta_{exp.} + b$) between calculated and experimental ^{51}V shifts, with a slope close to unity (0.97), an almost zero intercept (–1 ppm) and a correlation coefficient of 0.999 (Figure 2). We attribute the observed improvement in δ calculations employing the model SAOP functional to the better estimation of the paramagnetic term, σ_p, which is in fact the predominant contribution to the isotropic ^{51}V shielding (Supporting Information, Tables S1–S3). As documented elsewhere,[26] the use of SAOP leads to an increase in the HOMO–LUMO gap, thus correcting the extremely large paramagnetic contribution, which has been identified to give deficient chemical shifts with GGA functionals, such as the BP one.

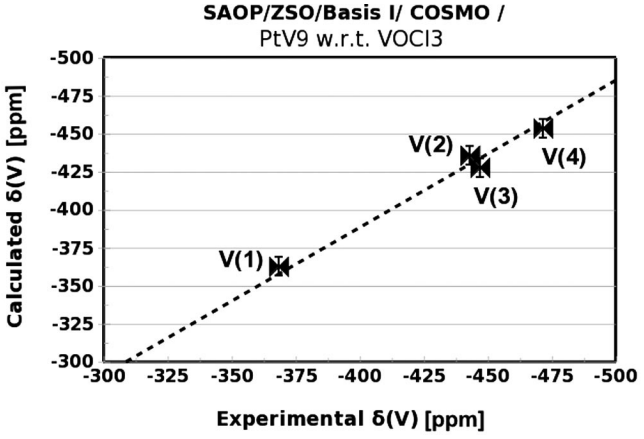

Figure 2. Correlation between calculated and experimental $\delta(^{51}V)$ values in $[H_2Pt^{IV}V_9O_{28}]^{5-}$ with respect to $VOCl_3$. COSMO calculations at *SAOP/ZORA spin-orbit/Basis I* level on COSMO-optimized geometry in water (*BP/ZORA scalar/Basis II/COSMO*). The correlation line ($\delta_{calcd.} = a\delta_{exp.} + b$) has $a = 0.97 \pm 0.02$, $b = -1 \pm 6$ ppm and $r^2 = 0.999$. Error bars indicate the standard error of the linear regression, $RSE = \pm 6.1$ ppm.

It should be noted, however, that SAOP occurs to be rather computationally expensive in the case of POMs. Our preliminary checks have shown that depending on the type and number of heavy nuclei involved in the POM structure, SAOP can be more than five times slower than the BP functional. Because the most valuable aid of the computational studies is drawing well-characterized correlations for accurate assignment and/or predictions of the NMR spectra of POMs, the level of theoretical treatment adopted, with respect to XC functional, basis set and inclusion of relativistic and solvent effects, should offer a good balance between performance and cost. In this vein, we would recommend the employment of too computationally expensive functionals only when the lower computational levels fail to give reasonable predictions.

It is seen from Table 1A that the strong deshielding caused by platinum, and its unequal effect on V1, V2 and V3, is reproduced in all the three computational series performed. However, the ordering of the signals for V2 and V3 (differing by only 4 ppm) is reversed, even after computation at the highest (*SAOP/ZSO/COSMO*) level. In this vein, it should be noted that the statistical error of the best correlation (Figure 2) is about 6% of the encompassed ^{51}V δ range of 103 ppm, that is, for peaks differing by less than 6 ppm, the statistical accuracy becomes questionable.

Dilacunary Polyoxotungstates

The next set of calculations is focused on a couple of dilacunary Keggin derivatives (Figure 1C) with interesting catalytic properties, namely, the decatungstosilicate $[\gamma\text{-}SiW_{10}O_{36}]^{8-}$, reported by Hervé and co-workers,[23] and its germanium analogue $[\gamma\text{-}GeW_{10}O_{36}]^{8-}$, synthesized in the group of Kortz.[22] In the crystal structure of these polyanions, the 10 tungsten atoms are nonequivalent, but in solution, the more symmetric conformation (C_{2v}) with three kinds of W nuclei is adopted, and the corresponding ^{183}W NMR spectrum presents three peaks with relative intensities 4:4:2.[22,23] The notation of the nonequivalent W atoms, corresponding to the assignment of the NMR signals, is depicted in Figure 1C, with the two W(C) nuclei being the most shielded and the four remote W(A) nuclei being the most deshielded ones.

The lacunary polyoxotungstates are computationally challenging not only because of the presence of a large number of W atoms, but more importantly, because the vacant sites in them are known to entail specific counterion and solvent effects.[13,30,31] As highlighted by Bagno et al.,[13] solution ^{183}W NMR spectra of the alkali-metal salts of lacunary polyoxotungstates may be interpreted as corresponding to either isolated anions, or to ion pairs in which the cation is specifically included in the lacuna. We followed this approach when considering the potassium salt of the decatungstogermanate whose experimental ^{183}W spectrum spans only 65 ppm. In Figure 3, the computed spectra of $[\gamma\text{-}GeW_{10}O_{36}]^{8-}$ and $[\gamma\text{-}KGeW_{10}O_{36}]^{7-}$ (with K^+ located at the centre of the lacuna of the optimized structure), as obtained after COSMO calculations, are compared to the experimental one for the K salt in water, by using W6O19 as a reference. It turns out that the ordering of the three resonances is reproduced in both series of calculations. However, in the spectrum of $[\gamma\text{-}KGeW_{10}O_{36}]^{7-}$, the arrangement of the W(B) and W(C) signals, though a bit shielded,

fits the experimental spectrum much better: the distance between the respective peaks is calculated almost equal to the experimental one ($\Delta\delta$ = 26 ppm vs. 29 ppm), whereas in the case of the isolated anion, $\Delta\delta$ between W(B) and W(C) is reduced to 19 ppm. Furthermore, the deviation from the experimental chemical shift values for W(B) and W(C) decreases by more than a factor of two if the lacuna of [γ-$GeW_{10}O_{36}]^{8-}$ is occupied by K^+ (see Figure 3 and the corresponding data in Table 1C). Thus, our calculations support the well-established fact[13,23] that the presence of a counterion in the lacuna modifies the chemical shifts of the polyanion, with the effect being mostly pronounced for the tungsten nuclei adjacent to the lacuna.

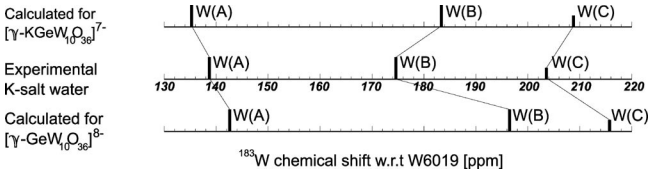

Figure 3. Bar graph ^{183}W NMR spectra of the dilacunary decatungstogermanate; see Figure 1 for assignment. All δ values with respect to $[W_6O_{19}]^{2-}$. Top to bottom: calculated spectrum for [γ-$KGeW_{10}O_{36}]^{7-}$; experimental spectrum for the K-salt in water[22] and calculated spectrum for the isolated anion [γ-$GeW_{10}O_{36}]^{8-}$. Nuclear shielding calculations are performed at *BP/ZORA spin-orbit/Basis II/COSMO* level on geometries optimized at *BP/ZORA scalar/Basis I/COSMO* level.

To explore the effect of the type of counterion on the ^{183}W NMR spectrum of dilacunary polyoxotungstates, we carried out calculations on a couple of [γ-$MXW_{10}O_{36}]^{7-}$ complexes, with X = Si or Ge and M = Li^+, Na^+ or K^+. The corresponding optimized structures (*BP/ZORA scalar/Basis II*) are depicted in Figure 1; the computed chemical shifts (relative to W6O19) as obtained after gas phase and COSMO calculations at *BP/ZORA spin-orbit/Basis II* level are listed in Table 1, parts B and C, respectively, along with the available experimental δ values relative to those of W6O19 and to WO4.

The "gas-phase" approach (in both geometry optimization and nuclear shielding calculations) yields a large MAE of 71 ppm across a δ range of only 84 ppm, embracing the whole set of [γ-$MXW_{10}O_{36}]^{7-}$ ions considered. The respective correlation between the computed and experimental $\delta(^{183}W)$ values (with respect to W6O19) has a slope smaller than unity (a = 0.7) and poor accuracy (RSE = ± 12 ppm; i.e., 14% of δ range), see Figure 4A.

If the solvent is taken into account, much better results are attained. We performed two series of COSMO calculations (*BP/ZORA spin-orbit/Basis II/COSMO*): in the first, we considered the [γ-$MXW_{10}O_{36}]^{7-}$ structures as optimized in continuous aqueous medium, whereas in the second one, besides embedding the complexes in the "continuum water", we located explicitly a water molecule in the vicinity of the alkali-metal cation occupying the POM lacuna (see the first two structures in Figure 1C). As seen from Table 1C, in the series of silicotungstates, the calculated chemical shifts of W(A) and W(B) in the $(H_2O)Li^+$ and

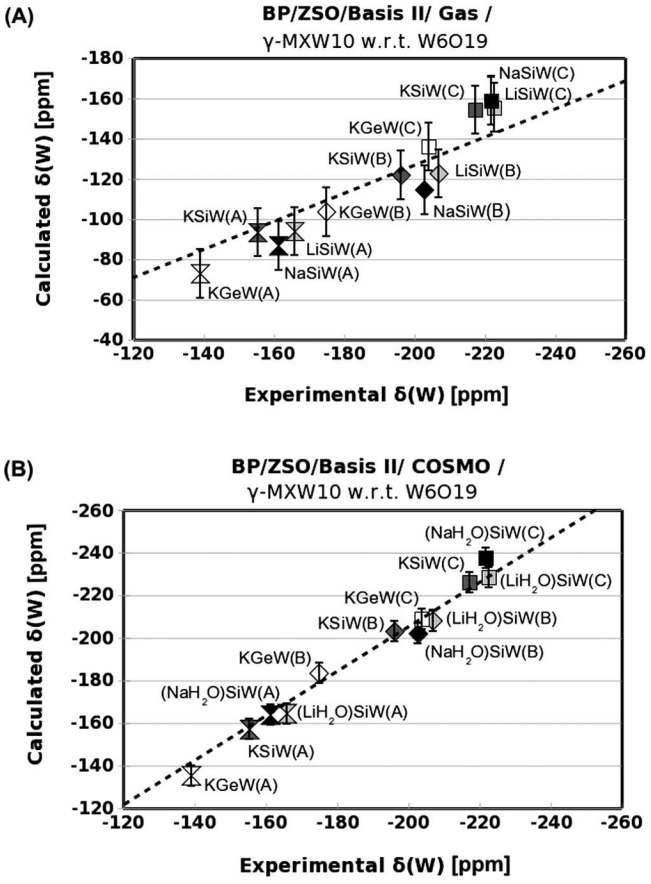

Figure 4. Correlation between calculated and experimental $\delta(^{183}W)$ values in [γ-$MXW_{10}O_{36}]^{7-}$, where X = Si or Ge, and M = Li^+, Na^+ or K^+. All δ values with respect to $[W^6O_{19}]^{2-}$. Correlation of the type $\delta_{calcd.} = a\delta_{exp.} + b$, with error bars indicating the standard error of the linear regression, RSE. (A) Gas-phase calculations (*BP/ZORA spin-orbit/Basis II/Gas*) on gas phase-optimized geometries (*BP/ZORA scalar/Basis I*); correlation line with a = 0.698 ± 0.059, b = 12.9 ± 10.8 ppm, r^2 = 0.928 and RSE = ± 12 ppm. (B) COSMO calculations in water (*BP/ZORA spin-orbit/Basis II/COSMO*) on COSMO-optimized geometries with an explicitly located H_2O molecule in the vicinity of Li^+ and Na^+ (*BP/ZORA scalar/Basis I/COSMO*); correlation line with a = 1.043 ± 0.024, b = 3 ± 4 ppm, r^2 = 0.994 and RSE = ± 4.8 ppm. Nuclei W(A) double triangles; nuclei W(B) diamonds; nuclei W(C) squares.

$(H_2O)Na^+$ inclusion complexes virtually coincide with the experimental δ values, whereas the shielding of W(C) is overestimated by 5 and 15 ppm, respectively. In contrast, in the case of the largest alkali-metal cation considered here, the inclusion of $(H_2O)K^+$ instead of only K^+ results in stronger overshielding of all tungsten nuclei in both the silico- and germanotungstates with respect to the experiment, and hence, to a worse computational output (see Table 1C). On the basis of these findings, the best agreement between calculated and experimental $\delta(^{183}W)$ values of the studied dilacunary decatungstates, with a MAE of only 5 ppm, is achieved by COSMO calculations on [γ-$(H_2O)LiSiW_{10}O_{36}]^{7-}$, [γ-$(H_2O)NaSiW_{10}O_{36}]^{7-}$, [γ-$KSiW_{10}O_{36}]^{7-}$ and [γ-$KGeW_{10}O_{36}]^{7-}$, underlining the importance of the polarization of the structures by the solvent. The corre-

sponding best correlation line (see Figure 4B) exhibits excellent fitting parameters (a = 1.04, b = 3 ppm and r^2 = 0.99) and accuracy that is improved more than twofold (*RSE* = ± 4.8 ppm; i.e., 6% of δ range) as compared to the "gas-phase" approach.

The effect of the type of the alkali-metal counterion on the ^{183}W NMR spectrum of the dilacunary decatungstogermanate anion was also modelled computationally, though by far, experimental δ values are available for its K salt[22] only. The comparison of the COSMO-calculated chemical shifts as obtained for $[\gamma\text{-}(H_2O)LiGeW_{10}O_{36}]^{7-}$, $[\gamma\text{-}(H_2O)NaGeW_{10}O_{36}]^{7-}$ and $[\gamma\text{-}KGeW_{10}O_{36}]^{7-}$ (by analogy with the $[\gamma\text{-}MSiW_{10}O_{36}]^{7-}$ series) is presented in Table 2. As a result of the calculations (*BP*/*ZORA spin-orbit*/*Basis II*/*COSMO* level), a consistent deshielding (from $\delta \approx -197$ to -183 ppm) with changing the counterion from Li^+ to K^+ is predicted only for the four W(B) nuclei adjacent to the lacuna (see Figure 1C for notation). For the remote W(A) and W(C) nuclei no such a trend was found: W(A) are computed to be a bit more deshielded (by 9 ppm) in $[\gamma\text{-}KGeW_{10}O_{36}]^{7-}$ than in $[\gamma\text{-}(H_2O)LiGeW_{10}O_{36}]^{7-}$ and $[\gamma\text{-}(H_2O)NaGeW_{10}O_{36}]^{7-}$, whereas W(C) are predicted to be mostly shielded in the Na salt and equally deshielded (by 8 ppm) in the case of Li^+ and K^+.

Table 2. Calculated ^{183}W NMR chemical shifts (*BP*/*ZORA spin-orbit*/*Basis II*/*COSMO*) of the dilacunary decatungstogermanate anion, as a function of the type of the alkali-metal counterion. The δ values are reported with respect to $[W_6O_{19}]^{2-}$. Calculations are carried out on geometries optimized at *BP*/*ZORA scalar*/*Basis I*/*COSMO* level.

Counterion of	Calculated ^{183}W δ [ppm] at BP/ZSO/Basis II/COSMO		
$[\gamma\text{-}GeW_{10}O_{36}]^{8-}$	W(A)	W(B)	W(C)
$(H_2O)Li^+$	–144.154	–196.939	–208.707
$(H_2O)Na^+$	–144.488	–188.143	–216.800
K^+	–135.493	–183.540	–208.997

Conclusions

A DFT approach with Slater-type basis, and inclusion of relativistic and solvent effects, was tested for NMR calculations on transition-metal centres in POMs. ^{51}V and ^{183}W chemical shifts for a monoplatinum decavanadate derivative and a set of dilacunary polyoxotungstates were calculated at several levels of theoretical treatment regarding solvent, counterion and exchange-correlation functional. We have shown that the use of a model SAOP functional in ZORA spin–orbit calculations with solvent effects included by COSMO, substantially improves the agreement between computed results and experimental benchmarks for ^{51}V chemical shifts (at least, in the case of $[H_2Pt^{IV}V_9O_{28}]^{5-}$). Our calculations support the idea that for accurate predictions of the ^{183}W NMR spectra of dilacunary polyoxotungstates one should model not only the solvent, but the presence of a counterion in the POM lacuna and its type, as well. We have found that if the counterion is relatively small (like Li^+ and Na^+), the explicit location of a water molecule in its vicinity (in addition to the overall COSMO treatment) improves the correlation between computed and experimental shifts even further. These findings encourage us to consider the computational NMR spectroscopy involving relativistic DFT calculations as a reliable methodology that can assist synthesis and structure development of novel POMs.

Experimental Section

Computational Details: All calculations were performed by density functional theory (DFT) as implemented in the Amsterdam density functional (ADF 2008) code.[17] We used all-electron (AE) as well as frozen-core (FC) basis sets, composed of singly polarized Slater functions of double-ζ (DZP) and triple-ζ (TZP) quality. Two combinations of basis sets, denoted as *Basis I* and *Basis II*, were adopted: (1) *Basis I* is a locally-dense all-electron basis combining DZP for the light elements (O, Si, Ge, H) and TZP for the heavy elements (Pt, W, V) and the alkali-metals (Li, Na, K); (2) *Basis II* is a combination of AE-TZP for the alkali-metals and AE-DZP for H and FC basis for W, Ge, Si and O with core shells defined as W.4d(TZP), Ge.3p(DZP), Si.2p(DZP), O.1s(DZP).

In accordance with previous studies,[4,13] we employed the Becke 88 exchange with the Perdew 86 correlation (BP) functional[24] in the geometry optimization and in most of the NMR calculations. In a series of calculations of ^{51}V chemical shifts we tested the so-called "statistical average of model orbital potentials" (SAOP) Kohn–Sham functional,[25] which has been found[26] to substantially increase the accuracy of the calculated chemical shifts for molecules containing light elements, with respect to the LDA and GGA potentials (like VWN and BP, respectively).

Relativistic corrections were always taken into account. In all cases, scalar relativistic corrections (ZSC) have been considered by means of the zeroth-order regular approximation (ZORA).[18,27–29] For higher accuracy calculations, we also included spin-orbit coupling (ZSO) in the Hamiltonian.

Solvent treatment was accomplished by the ADF implementation[17,20] of the conductor-like screening Model (COSMO)[21] for water (ε = 78.4).

The computational procedure starts with optimization of the POM geometry. The importance of this step stems from the fact that structural determination by experimental techniques (e.g., X-ray diffraction analysis) is not always possible.[22] Moreover, it is well known[23] that in solution polyanions exhibit a more symmetric conformation than the one which is determined by XRD for crystalline samples. Because the experimental ^{51}V and ^{183}W NMR spectra are measured in solution, it is important to run the calculations on the proper POM geometries. All optimizations were performed by taking full advantage of symmetry at the *BP*/*ZORA scalar*/*Basis I* level in either gas phase, or in continuum water (by means of COSMO).

NMR calculations are preceded by the electron density computation (Single Point), which was carried out at five different levels, as follows: (1) *BP*/*ZSO*/*Basis I* on gas phase geometry; (2) *BP*/*ZSO*/*Basis I*/*COSMO* on geometry in water; (3) *SAOP*/*ZSO*/*Basis I*/*COSMO* on geometry in water, all in the case of $[H_2Pt^{IV}V_9O_{28}]^{5-}$ and (4) *BP*/*ZSO*/*Basis II* on gas phase-geometry; (5) *BP*/*ZSO*/*Basis II*/*COSMO* on geometry in water, both in the case of the $[\gamma\text{-}MXW_{10}O_{36}]^{7-}$ series.

The ADF *nmr* property module enables calculation of nuclear shieldings.[17] For the POMs considered here, shielding calculations

were carried out at the ZORA spin-orbit level (ZSO), and the isotropic shielding constant σ is given in this case by the sum of the diamagnetic, paramagnetic and spin–orbit contributions ($\sigma = \sigma_d + \sigma_p + \sigma_{SO}$). Computed chemical shifts, $\delta_{calcd.}$, were then determined by the difference between the shielding of a reference standard, σ_{ref}, (for which $\delta = 0$ ppm) and the shielding of the nucleus of interest, σ, as $\delta_{calcd.} = \sigma_{ref} - \sigma$. Vanadium chemical shifts for $[H_2Pt^{IV}V_9O_{28}]^{5-}$ were calculated with respect to $VOCl_3$, which is the accepted reference of experimental ^{51}V NMR spectroscopy. In the case of ^{183}W NMR the choice of a proper reference for accurate δ calculations is a bit complicated. As shown by Bagno et al.,[4] the experimental chemical shift standard, aqueous WO_4^{2-} (WO4), exhibits entirely different electronic structure and response to solvent, as compared to a large set of polyoxotungstates of various structural groups. In fact, much better consistency between computed and experimental δ values was achieved by using as a reference the Lindqvist polyanion $[W_6O_{19}]^{2-}$ (W6O19), which resonates at $\delta = 58.9$ ppm with respect to WO4.[4] Following those findings, all ^{183}W δ values for the series of polyoxotungstates considered here are reported with respect to W6O19 (see Table 1B and C).

As mentioned in the Introduction, the performance of the adopted computational procedure is assessed with respect to the experimental data by two parameters: (1) the mean absolute error (MAE) as proposed by Bagno et al.[4] and (2) the standard error of the linear regression (*RSE*) defined as:

$$RSE = \sqrt{\frac{1}{n-2}\sum_{i=1}^{n}(\delta_{calcd.} - \delta_{pred.})_i^2}$$

where n is the number of samples considered and $\delta_{pred.}$ denotes the predicted chemical shift values with fitting parameters from the best correlation between the corresponding calculated and experimental δ values.

Supporting Information (see footnote on the first page of this article): Supporting Information contains Cartesian coordinates of the optimized geometries, values of the isotropic shielding constant and its individual contributions as calculated at all the computational levels employed, as well as correlation plots not included in the main paper.

Acknowledgments

The German Science Foundation (DFG) is gratefully acknowledged for a visiting research grant. N.V. also thanks Dr. L. Zhechkov from the Theoretical Physics/Theoretical Materials Science group at Jacobs University Bremen for his valuable comments, suggestions and help with preparation of some of the figures.

[1] D.-L. Long, E. Burkholder, L. Cronin, *Chem. Soc. Rev.* **2007**, *36*, 105–121, and references therein.
[2] J. J. Borras-Almenar, E. Coronado, A. Mueller, M. T. Pope (Eds.), *Polyoxometalate Molecular Science*, Kluwer, Dordrecht, The Netherlands, **2004**.
[3] M. T. Pope, *Inorganic Chemistry Concepts Vol. 8: Heteropoly and Isopoly Oxometalates*, Springer, Berlin, **1983**.
[4] A. Bagno, M. Bonchio, J. Autschbach, *Chem. Eur. J.* **2006**, *12*, 8460–8471.
[5] U. Lee, H.-Ch. Joo, K.-M. Park, S. S. Mal, U. Kortz, B. Keita, L. Nadjo, *Angew. Chem. Int. Ed.* **2008**, *47*, 793–796.
[6] M. A. Fedotov, R. I. Maksimovskaya, *J. Struct. Chem.* **2006**, *47*, 952–978.
[7] J. Ed. Mason, *Multinuclear NMR spectroscopy*, Plenum, New York, **1987**.
[8] A. Bagno, G. Saielli, *Theor. Chem. Acc.* **2007**, *117*, 603–619.
[9] B. M. Still, P. G. A. Kumar, J. R. Aldrich-Wright, W. S. Price, *Chem. Soc. Rev.* **2007**, *36*, 665–686.
[10] Y.-G. Chen, J. Gong, L.-Y. Qu, *Coord. Chem. Rev.* **2004**, *248*, 245–260.
[11] A. Bagno, G. Scorrano, *Acc. Chem. Res.* **2000**, *33*, 609–616.
[12] F. Jensen, *Introduction to Computational Chemistry*, Wiley, Chichester, **1999**.
[13] A. Bagno, M. Bonchio, A. Sartorel, G. Scorrano, *ChemPhysChem* **2003**, *4*, 517–519.
[14] M. Kaupp, M. Buehl, V. G. Malkin (Eds.), *Calculation of NMR and EPR Parameters*, Wiley-VCH, Weinheim, **2004**.
[15] J. Autschbach in *Principles and Applications of Density Functional Theory in Inorganic Chemistry I* (Eds.: N. Kaltsoyannis, J. E. McGrady), Springer, Heidelberg, **2004**, vol. 112, p. 1.
[16] J. Autschbach, T. Ziegler in *Encyclopedia of Nuclear Magnetic Resonance* (Eds.: D. M. Grant, R. K. Harris), Wiley, Chichester, **2002**, vol. 9, p. 306.
[17] a) G. te Velde, F. M. Bickelhaupt, E. J. Baerends, C. Fonseca Guerra, S. J. A. van Gisbergen, J. G. Snijders, T. Ziegler, *J. Comput. Chem.* **2001**, *22*, 931–967; b) ADF 2008.01, ADF User's Guide, http://www.scm.com, SCM, Theoretical Chemistry, Vrije Universiteit, Amsterdam; c) http://www.cobalt.chem.ucalgary.ca/ziegler/Chem575/Lab/Lab9.html.
[18] J. Autschbach in *Calculation of NMR and EPR Parameters* (Eds.: M. Kaupp, M. Buehl, V. G. Malkin), Wiley-VCH, Weinheim, **2004**, ch. 14, p. 227.
[19] J. Autschbach, T. Ziegler in *Calculation of NMR and EPR Parameters: Theory and Applications* (Eds.: M. Kaupp, M. Buehl, V. G. Malkin), Wiley-VCH, Weinheim, **2004**, ch. 15, p. 249.
[20] C. C. Pye, T. Ziegler, *Theor. Chem. Acc.* **1999**, *101*, 396–408.
[21] a) A. Klamt, G. Schuurmann, *J. Chem. Soc. Perkin Trans. 2* **1993**, 799–805; b) A. Klamt, V. Jones, *J. Chem. Phys.* **1996**, *105*, 9972–9981; c) A. Klamt, *J. Phys. Chem.* **1995**, *99*, 2224–2235.
[22] N. H. Nsouli, B. S. Bassil, M. H. Dickman, U. Kortz, B. Keita, L. Nadjo, *Inorg. Chem.* **2006**, *45*, 3858–3860.
[23] J. Canny, A. Tézé, R. Thouvenot, G. Hervé, *Inorg. Chem.* **1986**, *25*, 2114–2119.
[24] a) A. D. Becke, *Phys. Rev. A* **1988**, *38*, 3098–3100; b) J. P. Perdew, *Phys. Rev. B* **1986**, *33*, 8822–8824.
[25] P. R. T. Schipper, O. V. Gritsenko, S. J. A. van Gisbergen, E. J. Baerends, *J. Chem. Phys.* **2000**, *112*, 1344–1352.
[26] J. Poater, E. van Lenthe, E. J. Baerends, *J. Chem. Phys.* **2003**, *118*, 8584–8593.
[27] S. K. Wolff, T. Ziegler, E. van Lenthe, E. J. Baerends, *J. Chem. Phys.* **1999**, *110*, 7689–7698.
[28] E. van Lenthe, E. J. Baerends, J. G. Snijders, *J. Chem. Phys.* **1993**, *99*, 4597–4610.
[29] E. van Lenthe, PhD Thesis, Vrije Universiteit, Amsterdam, **1996**.
[30] J. F. Kirby, L. C. W. Baker, *Inorg. Chem.* **1998**, *37*, 5537–5543.
[31] V. A. Grigoriev, D. Cheng, C. L. Hill, I. A. Weinstock, *J. Am. Chem. Soc.* **2001**, *123*, 5292–5307, and references cited therein.

Received: September 27, 2009
Published Online: October 29, 2009

